Available online at www.sciencedirect.com
ScienceDirect
Ceramics International 37 (2011) 2175–2180
CERAMICS INTERNATIONAL
www.elsevier.com/locate/ceramint

Effect of heating rate on microstructure and properties of spark plasma sintered Li-α-sialon

Zhangfu Yang [a], Hao Wang [a,*], Xinmin Min [a], Weimin Wang [a], Zhengyi Fu [a], Soo Wohn Lee [b], Koichi Niihara [c]

[a] State Key Lab of Advanced Technology for Materials Synthesis and Processing, Wuhan University of Technology, Wuhan 430070, China
[b] Department of Environmental Engineering, Sun Moon University, Chungnam 336-708, Republic of Korea
[c] Extreme Energy-Density Research Institute, Nagaoka University of Technology, 1603-1 Kamitomioka, Nagaoka, Niigata 940-2188, Japan

Received 14 January 2011; received in revised form 25 February 2011; accepted 3 March 2011
Available online 9 March 2011

Abstract

Li-α-sialon ceramics with low oxygen content were prepared by spark plasma sintering at 1750 °C, using three heating rates of 100 °C/min, 200 °C/min and 300 °C/min. In all cases, the densification of Li-α-sialon ceramics is effectively promoted. The rapidly anisotropic growth of grains, either α-sialon or β-sialon, is significantly enhanced with a heating rate above 200 °C/min. This could be attributed to a large amount of low viscosity oxygen-rich liquid formed at elevated temperatures, which gives rise to a so-called dynamic ripening mechanism at the early stage of sintering. Furthermore, for the composition near α-sialon boundary, the oxygen-rich liquid results in the formation of β-sialon together with a large amount of intergranular glassy phase. Only the Li-doped sialon with low lithium and oxygen content possesses relatively high infrared transmittance when sintered at a rate of 100 °C/min.

Keywords: A. Sintering; B. Microstructure-final; C. Optical properties; D. Sialon

1. Introduction

The α-sialon (abbreviated as α′) ceramics, solid solutions of α-Si_3N_4, have been extensively studied for structural applications due to their excellent mechanical properties, chemical stability and heat resistance [1]. α′ is generally formulated as $M_xSi_{12-m-n}Al_{m+n}O_nN_{16-n}$, where M stands for the stabilizing cation, being Li^+, Ca^{2+}, Mg^{2+}, or rare earth cations [2]. In comparison with α-Si_3N_4, the amount of intergranular glassy phase in the final α′ product can be greatly reduced by the incorporation of stabilizer into the α-Si_3N_4 matrix during transient liquid sintering [2].

Recently, more attention has been paid to the optical properties of α′ ceramics. The translucent α′ ceramics doped by various cations (e.g., Y^{3+}, Yb^{3+}, Lu^{3+}, etc. [3–7]) have been fabricated with high infrared transmittance so far. It is expected that the application field of α′ ceramics would be extended because of the combination of good high-temperature strength and optical transparency. However, these α′ ceramics, stabilized with rare earth cations, were commonly densified at very high temperatures (mostly not lower than 1800 °C [5,8] and even up to 1950 °C [6]) due to high viscosity of rare earth-containing aluminosilicate liquid. Moreover, in most cases, rare earth cations readily result in selective absorption in the infrared range owing to the special electron transition [5,7,9], which greatly decreases the transmittance of α′ in the corresponding wavelength range.

Compared with rare earth-doped α′, the full densification of Li-α′ could be achieved at a relatively lower temperature because of the lower eutectic melting point of Li_2O–Al_2O_3–SiO_2 (i.e., 1050 °C) [10]. The issue regarding selective absorption, furthermore, can be inherently avoided in Li-α′. Whereas, the volatilization of Li_2O during heating makes it difficult to realize full densification of Li-α′, especially with low oxygen content [10]. Sparking plasma sintering (SPS), a rapid sintering technique, enables us to consolidate fully dense ceramics within a few minutes. By this method, most recently, we have first reported that Li-α′ ceramic with equiaxed grains

* Corresponding author. Tel.: +86 027 87867824; fax: +86 027 87215421.
E-mail address: shswangh@whut.edu.cn (H. Wang).

0272-8842/$36.00
doi:10.1016/j.ceramint.2011.03.014

possesses relatively high infrared transmission when a heating rate of 100 °C/min is applied [11]. It has been proved that a high heating rate (i.e., 100 °C/min) prominently retards the Li_2O volatilization [12]. At the same time, such a rapid heating rate also has a pronounced impact on the microstructure of α′ and thereby influences the optical properties of α′. In the case of SPS, Shen et al. [13] prepared Yb-α′ ceramics with a tough interlocking microstructure at a heating rate of 200 °C/min, in contrast to equiaxed-grain morphology formed at 40 °C/min. However, there are few reports on the relationship between heating rate and the microstructure of Li-α′. In the present work, the influence of heating rate from 100 °C/min to 300 °C/min on the microstructure of Li-α′ was studied. The mechanical and optical properties of Li-α′ were investigated as well.

2. Experimental

To reduce the amount of residual glassy phase that severely deteriorates the optical properties of α′, two compositions with low oxygen content ($m = 0.6$, $n = 1.0$, and $m = 1.0$, $n = 1.0$, named as L06 and L10, respectively) were selected. They are located inside the single-phase region of the α′ plane represented by the formula $Li_xSi_{12-m-n}Al_{m+n}O_nN_{16-n}$. The former is near to the boundary between single-phase α′ and the two-phase α-sialon/β-sialon (β-sialon being abbreviated as β′) regions and the latter is toward the middle of α′ region, as presented in Fig. 1. The starting powders were α-Si_3N_4 (E10, Ube Industries, Tokyo, Japan), AlN (F grade, Tokuyama Co., Soda, Japan), and Li_2CO_3 (Shanghai chemical, Shanghai, China). The residual oxygen content in α-Si_3N_4 and AlN powders was taken into account in the composition formulation. The powders, in batches of 50 g, were ball milled in water-free ethanol for 24 h using Si_3N_4 milling media. They were subsequently dried at 60 °C in a rotary evaporator and sieved through a 325-mesh sieve. Powder mixtures were loaded in a BN-coated graphite die with a diameter of 15 mm and sintered in an SPS apparatus (Model 1050, Sumitomo Coal Mining Co. Ltd., Kanagawa, Japan) under a uniaxial pressure of 30 MPa in a 0.1 MPa nitrogen atmosphere. The samples were heated from ambient temperature to 600 °C within 2 min, then at 100 °C/min up to 1000 °C; a holding time of 1 min at 1000 °C was applied to ensure full densification. Three heating rates of 100, 200 and 300 °C/min were performed between 1000 °C and the sintering temperature of 1750 °C. The samples were naturally cooled inside the furnace after a soaking time of 5 min. The sintered samples were designated by the m value and the heating rate, e.g., the sample with $m = 0.6$ and $n = 1.0$ sintered at 100 °C/min was referred to as L06-1.

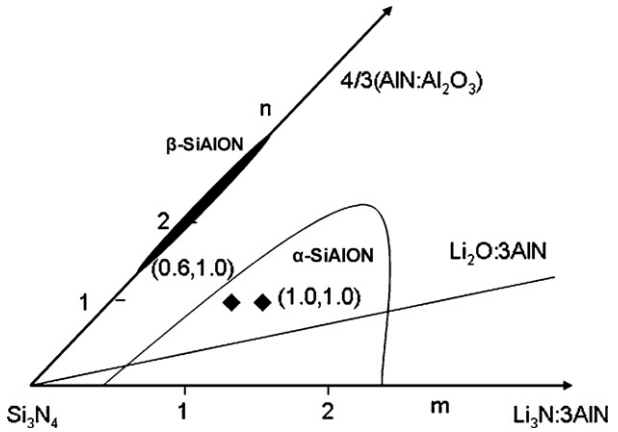

Fig. 1. Schematic phase diagram of Li-α-sialon plane showing the compositions used in this study.

The obtained samples were ground and then polished on both sides. The bulk density of the samples was measured by the Archimedes principle. Phase analysis was conducted by X-ray diffraction (XRD; Model D/MAX-RBX, Rigaku Co., Tokyo, Japan) with CuKα radiation. Lattice parameters were determined by XRD using Si as an internal standard and calculated by the software Unitcell. The actual x value of α′ was determined according to the formula reported by Hampshire et al. [2]. Microstructure was characterized by scanning electron microscopy (SEM; S-3400, Hitachi, Japan) after the samples were etched in molten NaOH for 60 s. To further observe intergranular glassy phase, transmission electron microscopy analysis (TEM; Model 2010F, JEOL, Tokyo, Japan) was also conducted. Vickers hardness and indentation fracture toughness were determined under a load of 98 N for 15 s.

3. Results and discussion

3.1. Bulk density, phase assemblage and lattice parameter

The bulk densities and phase assemblages of all the sintered samples are listed in Table 1. As shown, all the samples achieved full densification after being sintered at 1750 °C for 5 min. This reveals that the rapid heating rate is beneficial to the densification of Li-doped sialon with low oxygen content relative to the previous hot-pressing result at a rate of 10 °C/min [11]. For composition $m = 0.6$ and $n = 1.0$, as expected, only single-phase Li-α′ was formed at a heating rate of 100 °C/min (sample L06-1 in Table 1). However, a small proportion of β′ was detected besides α′ as the heating rate was higher than 100 °C/min. It should be noted that the appearance of β′ in samples sintered at heating rates above 200 °C/min could not be attributed to the Li_2O volatilization, since the Li_2O volatilization was significantly retarded within a longer heating time in the case of 100 °C/min. In contrast, no β′ was found in all L10 samples (composition $m = 1.0$, $n = 1.0$) in addition to α′. The XRD results illustrate that the influence of heating rate on phase assemblages is dependent on the overall composition of Li-doped sialon.

Table 1 also lists the lattice parameters of α′ in six samples. For $m = 0.6$ and $n = 1.0$, the a value slightly increases when the rate is increased from 100 °C/min to 200 °C/min and then remains constant with the further increase of heating rate. The calculated x values in L06-2 and L06-3 are about 0.62, which is larger than the nominal one of 0.6. The difference presumably results from the presence of small amounts of β′. For the both samples, the precipitation of β′ phase (containing no stabilizing cation) from the Li–Si–Al–O–N liquid makes the liquid richer

Table 1
Density, phase assemblage and α-sialon lattice parameter of the samples sintered at different heating rates with 5 min holding time.

Sample	Heating rate (°C/min)	Phase assemblage[b]		Density (g/cm^3)	Lattice parameter of α-sialon		
		α′	β′		a (Å)	c (Å)	x_{actual}
L06-HP[a]	10	vs		2.87	7.7922(6)	5.6587(1)	0.53
L06-1	100	vs		3.12	7.7953(4)	5.6602(1)	0.59
L06-2	200	vs	w	3.12	7.7971(7)	5.6606(1)	0.62
L06-3	300	vs	w	3.11	7.7974(8)	5.6600(3)	0.63
L10-1	100	vs		3.11	7.8049(3)	5.6677(2)	0.80
L10-2	200	vs		3.11	7.8053(5)	5.6669(1)	0.80
L10-3	300	vs		3.12	7.8051(6)	5.6672(2)	0.80

[a] HP, hot pressing; the results of L06-HP are from Ref. [11].
[b] X-ray intensities: vs, very strong; w, weak.

in lithium, and therefore, the incorporation of more Li^+ into α′ crystalline lattice is possible according to simple Le Chatelier's principle. At the same time, a large amount of intergranular glassy phase was formed along with the formation of β′, as described in Section 3.2. Compared with L06, either the a or c value is almost invariable in all L10 samples, showing that the level of the incorporation of Li^+ in this composition is not influenced by heating rate. The actual x value of ∼0.8 is less than the nominal one of 1.0 in L10 samples, suggesting that some of Li^+ do not enter the crystalline lattices and is probably left as Li-containing glassy phase at grain boundaries. Therefore, the effect of heating rate on lattice parameters of Li-α′ is also dependent on the overall composition.

3.2. Microstructure

The surface morphologies of the etched samples are given in Fig. 2. For $m = 0.6$ and $n = 1.0$, a large number of typically equiaxed grains with a size of ∼1 μm are observed in the sample heated at 100 °C/min and no elongated grains are found. Moreover, a very little amount of glassy phase remains at the grain boundaries [11]. However, at a rate of 300 °C/min, a small number of elongated grains with aspect ratios of 3–5 embedded in the fine equiaxed grains are characterized, as shown in Fig. 2(b). At the intermediate rate, i.e., 200 °C/min, the obtained microstructure is quite similar to that at 300 °C/min. This implies that the influence of heating rate on the microstructure decreases sharply when the heating rate exceeds 200 °C/min. Combined with XRD results, the elongated grains are confirmed as β′, which can be much more readily developed into elongated grains than α′. Generally, it is very difficult to estimate the amount of Li-containing glassy phase from the SEM-EDS micrograph. However, Peng et al. [12] considered that Li-α′ with a large amount of glassy phase was easily etched and many grains would drop off from the matrix after etching. In comparison with L06-1, the etched surface morphology in

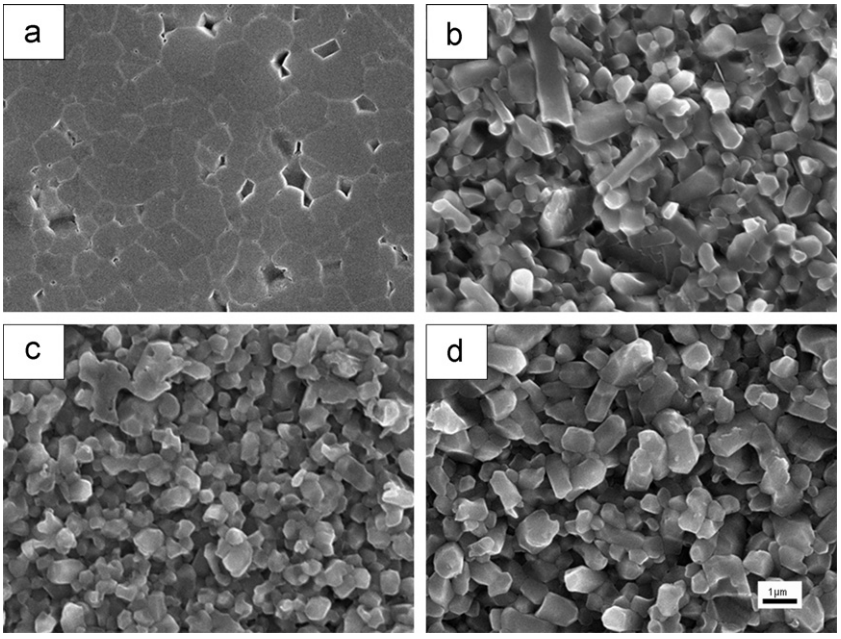

Fig. 2. SEM micrographs of the $m = 0.6$, $n = 1.0$ samples heated at heating rates of (a) 100 °C/min and (b) 300 °C/min, and the $m = 1.0$, $n = 1.0$ ones at (c) 100 °C/min and (d) 300 °C/min. The samples were sintered at 1750 °C for 5 min and etched in NaOH before SEM observation.

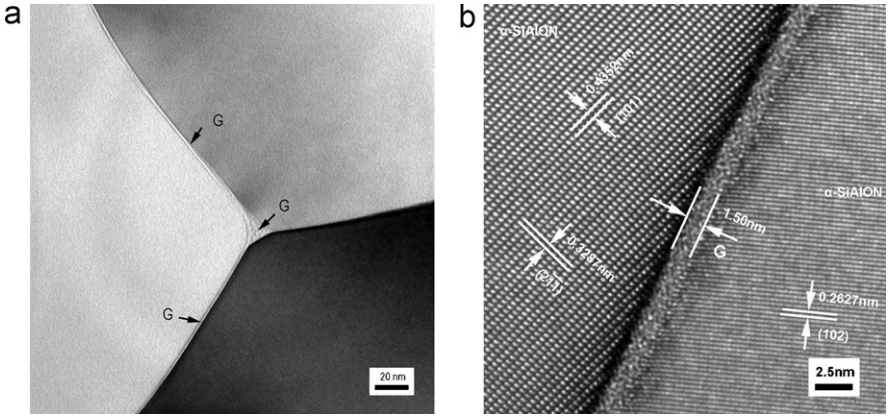

Fig. 3. TEM micrographs of the $m = 0.6$, $n = 1.0$ sample sintered at a heating rate of 300 °C/min showing (a) residual glassy phase at triple grain junction and (b) amorphous grain boundary film with about 1.5 nm ("G" denotes the glassy phase).

L06-2 or L06-3 is much closer to that of fractured surface, indicating that there is a large amount of intergranular glassy phase in these two samples. To directly observe intergranular glassy phase, transmission electron microscopy of the $m = 0.6$, $n = 1.0$ sample sintered at a rate of 300 °C/min was performed. As given in Fig. 3, residual amorphous phase at triple grain junctions and vitreous grains boundary film with about 1.5 nm can be characterized.

Compared with L06-1, L10-1 contains finer equiaxed grains with a size of about 500 nm and a few elongated grains with low aspect ratio, as given in Fig. 2(a). In general, the driving force for the transformation from α-Si_3N_4 to α′ is much higher in the composition toward the center of α′ region than near the boundary [14]. Thus the finer grains in L10-1 can be explained by the concept that the higher driving force yields the rapider nucleation rate. Whereas, it can be seen from the fracture-like morphology of L10-1 that a large amount of residual glassy phase exists at the grain boundaries, which is in accordance with the actual solubility $x = 0.8$. This implies that the Li-richer composition (L10 containing more Li than L06) readily leads to more liquid/glassy phase. Hence, the amount of residual glassy phase is also closely associated with the stabilizing cation content. The SEM morphologies of both L10-3 (presented in Fig. 2(d)) and L10-2 are very similar to that of L06-3. However, the elongated grains in either L10-2 or L10-3 are identified to be α′ instead of β′ in terms of the XRD results. As mentioned above, anisotropic growth of α′ grains is also promoted by a rate of 200 °C/min or higher.

Table 2
Mechanical properties of the samples heated at different rates with 5 min holding time.

Sample	Heating rate (°C/min)	Hardness (GPa)	Fracture toughness (MPa $m^{1/2}$)
L06-1	100	20.1 ± 0.2	3.0 ± 0.1
L06-2	200	19.4 ± 0.1	3.6 ± 0.1
L06-3	300	19.3 ± 0.2	3.6 ± 0.2
L10-1	100	20.3 ± 0.2	3.2 ± 0.2
L10-2	200	20.0 ± 0.2	3.5 ± 0.1
L10-3	300	20.4 ± 0.1	3.6 ± 0.2

3.3. Mechanical and optical properties

Table 2 lists the mechanical properties of these samples. As shown, all the samples have high hardness except for those containing a small amount of β′ grains. The fracture toughness is slightly improved in the samples containing elongated α′ or β′ grains. However, the highest fracture toughness is no more than 3.6 MPa $m^{1/2}$ as a result of the small amount and low aspect ratio of elongated grains. Although all the samples are fully densified after soaking for 5 min, only L06-1 exhibits relatively high infrared transmission with the maximum value of 57% at 1.4 μm [11], and the others are black in color. Fig. 4 indicates the optical photographs of L06-1 and L06-3, where the underlying text only under L06-1 is visible. The abrupt loss of transmission in the other samples could be ascribed to a great amount of residual glassy phase left at the grain boundaries, which is caused by the higher heating rate and/or higher Li content. Therefore, to obtain high infrared transmittance of α′ materials, glassy phase at grain boundaries should be reduced as far as possible.

3.4. Oxygen-rich liquid and dynamic ripening

To further clarify the reason for the anisotropic growth of α′ and β′ grains, other experiments were performed. The green bodies of the two compositions were sintered at 1750 °C with a heating rate of 300 °C/min, but the holding time was 0 and 1 min, respectively. In all cases, full densification was achieved in the sintered samples and the phase assemblages obtained were similar to that of the corresponding samples. However, for composition either $m = 0.6$, $n = 1.0$ or $m = 1.0$, $n = 1.0$, the sintered samples without holding consists mostly of fine equiaxed grains, as indicated in Fig. 5(a). While the samples after soaking for 1 min exhibits very similar morphologies to L10-3 (see Fig. 5(b)). This suggests that the process of fast development of elongated grains can be fulfilled approximately within 1 min no matter what composition is used, and the extended holding has a negligible impact on the anisotropic growth of grains. The results are consistent with the observation in rare earth systems [13].

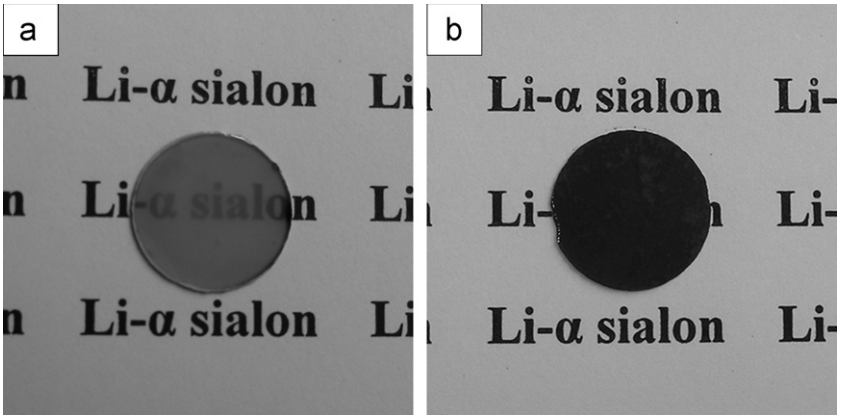

Fig. 4. Optical photographs of the $m = 0.6$, $n = 1.0$ samples sintered at heating rates of (a) 100 °C/min and (c) 300 °C/min, respectively.

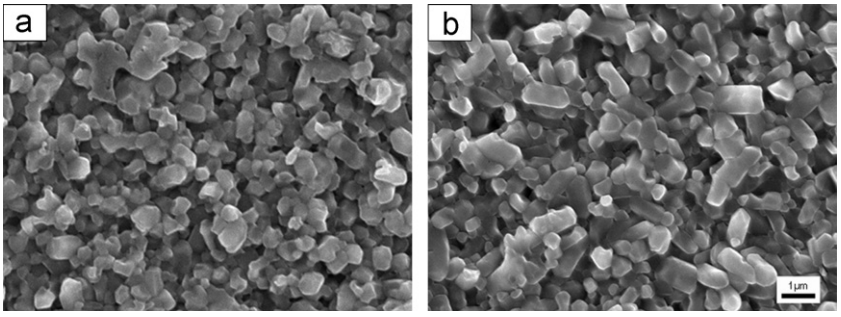

Fig. 5. SEM micrographs of the $m = 0.6$, $n = 1.0$ samples sintered at a rate of 300 °C/min with holding time of (a) 0 min and (b) 1 min, respectively.

During the formation of α′, the amount and viscosity of transient liquid could be strongly influenced by heating rate, as indicated by Zhang et al. [15] and Zenotchkine et al. [16]. When a rapid heating rate is used, the precipitation of α′ is delayed to elevated temperature. Thus more liquid exists at sintering temperature, which is beneficial to anisotropic growth of α′ grains. For example, Shen et al. [13] reported the in situ toughened Yb-α′ with elongated grains sintered at a rate of 200 °C/min by SPS. Furthermore, it has been proposed that the oxygen-rich liquid at low temperature is postponed to high temperature in the case of high heating rate [17]. Accordingly this liquid possesses a low viscosity. In this work, the fast development of elongated grains in samples L10-2 and L10-3 is believed to be promoted by a large amount of low viscosity oxygen-rich liquid. The serious unequilibrated liquid leads to a so-called dynamic ripening mechanism at the early stage of grain growth [13], which enhances the fast growth of elongated α′ grains. Simultaneously, the oxygen-rich liquid is rapidly exhausted and immediately rich in nitrogen, and then the driving force for the α-Si_3N_4 to α′ transformation is also reduced quickly. As soon as the liquid in the compact approaches thermodynamic equilibrium, the typical Ostwald ripening would govern the grain growth and lead to the instantly decreasing growth rate.

For composition $m = 0.6$, $n = 1.0$, the anisotropic growth of β′ grains, as such, is dominated by the dynamic ripening in the case of 200 °C/min or higher. Compared with $m = 1.0$, $n = 1.0$, the composition $m = 0.6$, $n = 1.0$ is much closer to the α′ + β′/α′ boundary. It can be understood that the high oxygen concentration around Si_3N_4 particles, especially with smaller size, easily makes the local composition shift from the single-phase α′ region to the duplex α′/β′ one. Hence, the formation of β′ can be explained. Furthermore, the β-Si_3N_4 particles existing in the α-Si_3N_4 raw material, which probably do not dissolve completely into the liquid in such a short time, can act as the heterogeneous nuclei to facilitate the precipitation of β′ [18]. Here, we first report that very high heating rate causes the formation of β′ in the composition located inside single-phase α′ region. The change in phase assemblage offers a forceful evidence for the supposal of oxygen-rich liquid present at high temperature. In most cases, this liquid phase itself seems to have little influence on the amount of residual glassy phase (e.g., in L10 samples), but it still results in the increase of glassy phase in some composition (e.g., in L06). Therefore, to achieve anticipant microstructure and/or high infrared transmittance in Li-α′ or even in other sialon systems, the heating rate should be carefully considered besides the overall composition.

4. Conclusions

The following conclusions can be drawn from the results of this study:

(1) The densification of Li-α-sialons with low oxygen content was promoted within a short time by spark plasma sintering at heating rates above 100 °C/min.
(2) When the heating rate exceeds a critical value (i.e., 200 °C/min), the oxygen-rich liquid delayed to higher temperature

would give rise to a so-called dynamic ripening mechanism, which enhanced the fast development of elongated grains. This process finishes approximately within a short time (i.e., 1 min) and then the following grain growth is subject to typical Ostwald ripening. In some cases, the oxygen-rich liquid results in the formation of other phases (e.g., β′).

(3) To obtain the expected microstructure and/or good optical properties in Li-α-sialon, appropriate heating rate should be considered in addition to the overall composition.

Acknowledgements

This research was financially supported by National Natural Science Foundation of China (A3 Foresight Program-50821140308), National High-Tech R&D Program of China (863 Program-No. 2007AA03Z527) and Specialized Research Fund for the Doctoral Program of Higher Education of China (SRFDP-No. 20090143110010).

References

[1] G.Z. Cao, R. Metselaar, α-Sialon ceramics: a review, Chem. Mater. 3 (1991) 242–252.
[2] S. Hampshire, H.K. Park, D.P. Thompson, K.H. Jack, α-Sialon ceramics, Nature 274 (1978) 880–882.
[3] H. Mandal, New developments in alpha-sialon ceramics, J. Eur. Ceram. Soc. 19 (1999) 2349–2357.
[4] M.I. Jones, H. Hyuga, K. Hirao, Optical and mechanical properties of alpha/beta composite sialons, J. Am. Ceram. Soc. 86 (2003) 520–522.
[5] F. Ye, L.M. Liu, C.F. Liu, H.J. Zhang, Y. Zhou, J. Yu, High infrared transmission of Y^{3+}–Yb^{3+}-doped α-sialon, Mater. Lett. 62 (2008) 4535–4538.
[6] M.I. Jones, H. Hyuga, K. Hirao, Y. Yamauchi, Highly transparent Lu-α-sialon, J. Am. Ceram. Soc. 87 (2004) 714–716.
[7] X.L. Su, P.L. Wang, W.W. Chen, B. Zhu, Y.B. Cheng, D.S. Yan, Translucent α-sialon ceramics by hot pressing, J. Am. Ceram. Soc. 87 (2004) 730–732.
[8] W.W. Chen, X.L. Su, P.L. Wang, D.S. Yan, Y.B. Cheng, K. Watari, Optical properties of Gd-α-sialon ceramics: effect of carbon contamination, J. Am. Ceram. Soc. 88 (2005) 2304–2306.
[9] Z.J. Shen, M. Nygren, U. Halenius, Absorption spectra of rare-earth-doped α-sialon ceramics, J. Mater. Sci. Lett. 16 (1997) 263–266.
[10] Z.B. Yu, Preparation of single phase lithium α-sialons, Brit. Ceram. Trans. 97 (1998) 41–47.
[11] Z.F. Yang, H. Wang, X.M. Min, W.M. Wang, Z.Y. Fu, S.W. Lee, K. Niihara, Translucent Li-α-sialon ceramics prepared by spark plasma sintering, J. Am. Ceram. Soc. 93 (2010) 3549–3551.
[12] H. Peng, Z.J. Shen, M. Nygren, Reaction sequences occurring in dense Li-doped sialon ceramics: influence of temperature and holding time, J. Mater. Chem. 13 (2003) 2285–2289.
[13] Z.J. Shen, Z. Zhao, H. Peng, M. Nygren, Formation of tough interlocking microstructures in silicon nitride ceramics by dynamic ripening, Nature 417 (2002) 266–269.
[14] A. Rosenflanz, I.-W. Chen, Kinetics of phase transformations in sialon ceramics: I. effects of cation size, composition and temperature, J. Eur. Ceram. Soc. 19 (1999) 2325–2335.
[15] C. Zhang, E. Narimatsu, K. Komeya, J. Tatami, T. Meguro, Control of grain morphology in Ca-alpha sialon ceramics by changing the heating rate, Mater. Lett. 43 (2000) 315–319.
[16] M. Zenotchkine, R. Shuba, I.-W. Chen, Effect of heating schedule on the microstructure and fracture toughness of alpha-sialon – cause and solution, J. Am. Ceram. Soc. 85 (2002) 1882–1884.
[17] Z.J. Shen, H. Peng, M. Nygren, Rapid densification and deformation of Li-doped sialon ceramics, J. Am. Ceram. Soc. 87 (2004) 727–729.
[18] S.L. Hwang, I.-W. Chen, Nucleation and growth of β-Sialon, J. Am. Ceram. Soc. 77 (1994) 1719–1728.